J Mater Sci (2011) 46:5512–5518
DOI 10.1007/s10853-011-5495-7

Effect of Nb and Nb_2O_5 additives on mechano-thermal processing of TiAl/Al_2O_3 nano-composite

S. Alamolhoda · S. Heshmati-Manesh · A. Ataie · S. Sheibani

Received: 29 November 2010 / Accepted: 21 March 2011 / Published online: 7 April 2011

Abstract In this research, TiAl matrix nano-composite with Al_2O_3 reinforcement was obtained by mechanical activation of TiO_2 and Al powder mixture and its subsequent heat treatment. Effect of Nb and/or Nb_2O_5 additions on the process was investigated. Structural changes and thermal behavior of the samples were evaluated by X-ray diffraction and differential thermal analysis, respectively. Moreover, the microstructure was characterized by transmission electron microscopy. The results confirmed the partial dissolution of Nb in Al during the milling stage in the Nb-added samples. The reaction mechanism during heat treatment in the sample without any additives was a two-stage process that was quite similar to the sample with Nb addition. However, Nb_2O_5 addition led to the progress of reaction through a single stage and with a higher rate. Both additives promoted formation of the Ti_3Al phase in the final products. The results confirmed the formation of nano-sized Al_2O_3 particles in a nano-crystalline Ti–Al matrix with a mean crystallite size of 30 nm.

Introduction

Intermetallic alloys based on γ-TiAl are potentially important class of engineering materials for various applications in the aerospace, gas turbine, and automotive industry, since they exhibit interesting properties such as relatively low density, high strength to weight ratio, good oxidation and corrosion resistance, and adequate creep resistance at high temperatures. However, they suffer from poor ductility, formability, and rapid crack growth rate at low temperatures [1–3]. Different reinforcements such as TiB_2 [4], Ti_5Si_3 [5], and SiC [6, 7] were used to strengthen the TiAl matrix. Development of in situ TiAl/Al_2O_3 composite may help to overcome the problems associated with the monolithic γ-TiAl alloys. In addition, the final phases in such a composite are thermodynamically compatible [7]. In situ TiAl/Al_2O_3 and/or Al_3Ti/Al_2O_3 composites have been already prepared by mechanical alloying and subsequent heat treatment of TiO_2 and Al powders by a number of research groups [8–14]. The following reaction may take place to form TiAl–Al_2O_3 composite:

$$3TiO_2 + 7Al \rightarrow 3TiAl + 2Al_2O_3 \qquad (1)$$

Microstructural control and alloying could also be used to improve γ-TiAl properties [15]. There are some studies on mechanical properties of TiAl alloys with different microstructures [16]. Mechanical properties such as ductility depend on both composition and microstructure of the material. Mechanical alloying has the possibility of microstructural modification and alloying in the solid state [15].

Different investigations have shown that addition of transition elements such as Nb, V, Cr, and Mn is highly effective on the properties of TiAl alloys produced by melting [17–20]. In addition, alloying elements have been added to binary Ti–Al alloys to increase the oxidation resistance [21]. It has been reported that Nb addition increases the strength, oxidation, and creep resistance of TiAl alloys as a result of solid solution strengthening, refinement of microstructure, and reduced stacking fault energy [1, 22, 23]. Furthermore, Nb is a α_2 (Ti_3Al) stabilizer in TiAl alloys. The presence of 0.05–0.015 vol.% of

S. Alamolhoda (✉) · S. Heshmati-Manesh · A. Ataie · S. Sheibani
School of Metallurgy and Materials Engineering, University of Tehran, P.O. Box 14395-553, Tehran, Iran
e-mail: alamhoda@ut.ac.ir

Ti_3Al phase in TiAl alloys has been shown to be beneficial since it is believed to refine the microstructure of these alloys and also acts as scavenger for N and O impurities preventing from precipitation of oxides and nitrides in TiAl matrix [17, 24].

This article thoroughly investigates the effect of Nb and Nb_2O_5 addition on processing of TiAl/Al_2O_3 nano-composite by mechanical alloying and subsequent heat treatment.

Experimental procedure

Starting materials in this study were commercially pure TiO_2 (<0.2 μm and 99.8 pct purity), Al (<100 μm and 99.8 pct purity), Nb (<30 μm and 99.9 pct purity), and Nb_2O_5 (<5 μm and 99.9 pct purity) powders. A mixture of Al and TiO_2 powders corresponding to Eq. 1 was milled up to 8 h in a Fritsch P6 type planetary ball mill with hardened steel balls and vial under high-purity argon gas. The milling speed was 300 rpm, and the ball-to-powder mass ratio was 20:1. Nb and/or Nb_2O_5 powders were added to the starting powder in a way that different contents of Nb exist in the metallic matrix of the final nano-composite. Table 1 summarizes the initial and final phase compositions of the samples.

The structure evolution in the powder mixture during milling and heat treatment stages was investigated by XRD (Philips PW-1730) using Cu Kα radiation.

Mean crystallite sizes of the milled powders and sintered samples were calculated by Cauchy–Gaussian approximation and Scherrer equation, respectively, using XRD patterns [25, 26]. The Cauchy–Gaussian approximation is known as:

$$\frac{\beta^2(2\theta)}{\tan^2\theta_0} = \frac{K\lambda}{L}\left[\frac{\beta(2\theta)}{\tan\theta_0 \sin\theta_0}\right] + 16e^2 \tag{2}$$

where θ_0 is the position of the analyzed peak maximum, λ is the X-ray wave length, L is the crystallite size, and e is the maximum strain. For all practical purposes, the constant K can be set equal to unity. $\beta(2\theta)$ should be calculated as the integral breadths rather than the FWHM, but this minor approximation introduces only a negligible difference. Any available orders of a given reflection may be used to construct a linear plot of $\beta^2(2\theta)/\tan^2(\theta_0)$ against $\beta(2\theta)/\tan(\theta_0)\mathrm{Sin}(\theta_0)$. From the slope ($\lambda/L$) and ordinate intercept $16e^2$, the crystallite size, L, and strain, e, may be determined.

The Scherrer equation is expressed as:

$$L = \frac{0.9\lambda}{\beta(2\theta)\mathrm{Cos}\theta_0} \tag{3}$$

where L is the mean crystallite size, $\beta(2\theta)$ is the breadth (commonly the FWHM or integral breadth) of the diffraction profile.

The lattice parameters were calculated using XRD data. The microstructure was evaluated in details by a Philips EM208S TEM operated at 100 kV. Thermal behavior of the milled powders was analyzed using DTA (Netzsch STA 409 PC/PG instrument) with a heating rate of 20 K/min up to 900 °C under flowing argon. Milled powders were cold pressed and heat treated for 1 h in a tube furnace under vacuum at 500 and 700 °C.

Table 1 The initial and final nominal compositions of the samples

Sample	Initial powder mixture	Final nominal composition
A	TiO_2–Al	TiAl–Al_2O_3
B1	TiO_2–Al–3 at.% Nb	TiAl–Al_2O_3–3 at.% Nb
B2	TiO_2–Al–5 at.% Nb	TiAl–Al_2O_3–5 at.% Nb
B3	TiO_2–Al–10 at.% Nb	TiAl–Al_2O_3–10 at.% Nb
B4	TiO_2–Al–15 at.% Nb	TiAl–Al_2O_3–15 at.% Nb
C1	TiO_2–Al–2.77 wt% Nb_2O_5	TiAl–Al_2O_3–3 at.% Nb
C2	TiO_2–Al–4.59 wt% Nb_2O_5	TiAl–Al_2O_3–5 at.% Nb
C3	TiO_2–Al–9.1 wt% Nb_2O_5	TiAl–Al_2O_3–10 at.% Nb
C4	TiO_2–Al–13.45 wt% Nb_2O_5	TiAl–Al_2O_3–15 at.% Nb

Results and discussion

Milling stage

Figure 1 shows XRD patterns of A, B3, and C3 samples milled for various times. The peaks tend to broaden as the milling time increases and their intensities decrease. This is due to the crystallite size refinement and increase in the level of lattice strain accumulation. No reaction between Al and TiO_2 could be detected even after 8 h of milling and only Nb and Nb_2O_5 peaks gradually vanished. Gradual disappearance of Nb and Nb_2O_5 peaks could be attributed to their refinement as a result of high energy ball milling. In addition, Nb atoms may be dissolved in Al matrix during the milling process. Similar results were also obtained for all the other milled samples, and hence their XRD patterns are skipped here.

To investigate the structural evolution and specially dissolution of Nb in Al in more detail, the calculated lattice parameter of Al in different samples as a function of Nb content is shown in Fig. 2. The results revealed that Nb_2O_5 additions do not change the Al lattice parameter, while Nb additions change the Al lattice parameter. This would reveal the partial dissolution of Nb in Al matrix. The formation of Al–25% Nb solid solution was previously reported in the mechanical alloying in Al–Nb system [27]. It could be seen that the most intensive lattice parameter

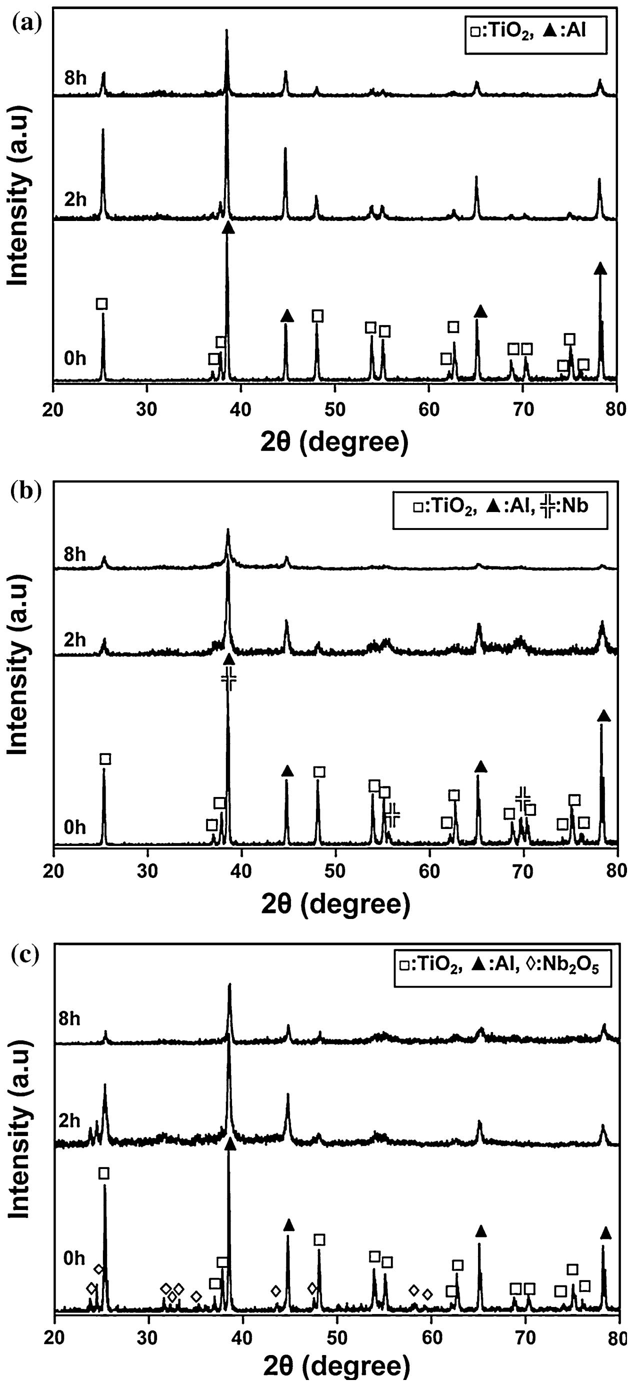

Fig. 1 XRD patterns of **a** A, **b** B3, and **c** C3 samples after different milling times

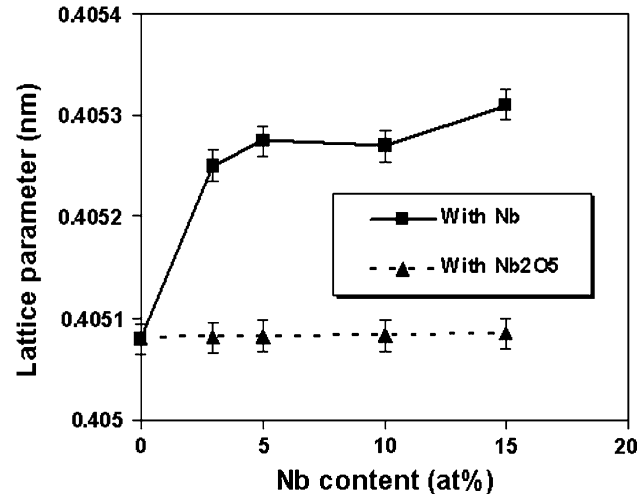

Fig. 2 Variation of Al lattice parameter as a function of composition in samples milled for 8 h in the presence of Nb and Nb_2O_5

increment occurs when the Nb content increases from 0 to 3 at% and further increase in Nb content has negligible effect on the Al lattice parameter.

Variation of the mean crystallite size of Al as a function of Nb content after 8 h of milling is shown in Fig. 3. It can be seen that Al crystallite size decreased by increasing the Nb content. Similar observation was also reported in the case of Zr addition to Al by Al-Aqeeli et al. [28]. This behavior seems to be due to the following reasons. It seems that Nb additions and its partial dissolution in Al matrix have probably changed the deformation mechanisms in mechanical alloying and introduced more defects into the Al crystals and resulted in more refinement. Furthermore, it is well known that the reduction in crystallite size during the milling process is the consequent of two processes; increment in density of defects as a result of exerted milling energy and dynamic recrystallization because of local temperature rise in the course of milling [29]. Reduced crystallite size as a result of Nb addition reveals that dissolution of Nb in the Al matrix is likely to increase the recrystallization temperature; therefore, it accelerates the crystallite size reduction. It was reported that Al–Nb bonding strength is higher than Al–Al bonding strength [30]. Therefore, dissolution of Nb increases the

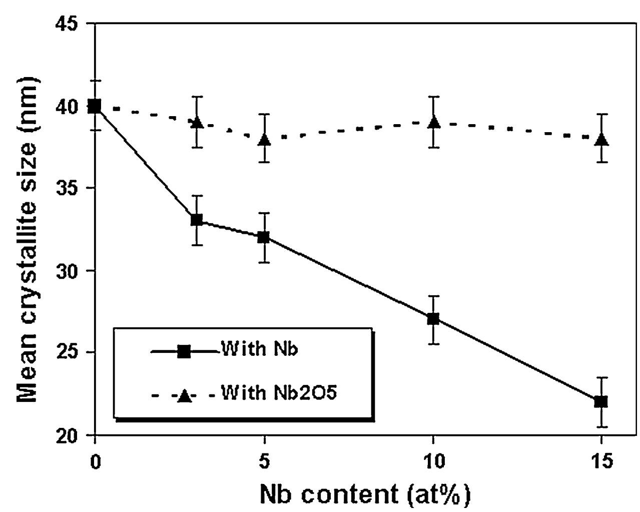

Fig. 3 Variation of Al mean crystallite as a function of composition in samples milled for 8 h in the presence of Nb and Nb_2O_5

re-crystallization temperature of Al by increasing the Al melting point.

Nb_2O_5 additions to the powder mixture seem to have no effect on Al crystallite size because Nb_2O_5 has no reaction with Al during the milling process.

Heat treatment stage

Thermal behavior of the milled materials was examined by DTA, and the results obtained from the samples A, B3, and C3 after 8 h of milling are shown in Fig. 4. The thermal analysis data are summarized in Table 2. Where, T_{on} is the onset reaction temperature, $T1_{max}$ and $T2_{max}$ are maximum reaction rate temperatures (peak temperatures), and A is the total peak area under DTA curve. DTA experiments followed by XRD investigations at different temperatures in Fig. 5 can provide more information regarding differences between different samples after 8 h of milling. However, superposition of some peaks related to the constituent elements introduces some complications in detail analysis of the system.

DTA traces reveal an exothermic peak in all the samples which is related to the aluminothermic reduction of TiO_2 by Al. XRD patterns in Fig. 5 indicate that the reaction is completed after heat treatment at 700 °C. It can be seen that the final product in all the samples comprises mainly of TiAl and Al_2O_3 together with a small amount of Ti_3Al. It should be noted that Ti_3Al content of the final product is increased in the presence of Nb in both B3 and C3 samples. However, ultra fine Nb particles distributed in the matrix are very difficult to be detected by the XRD technique.

DTA results also show that the onset temperature of the reaction in all three samples is the same. However, the DTA curves continued differently which could be related to the formation of intermediate phases. In the DTA trace of sample A shown in Fig. 4a, an exothermic reaction begins at about 540 °C which seems to be a combination of two overlapped exothermic peaks. The first peak with $T1_{max}$ of 584 °C corresponds to the reaction between the starting materials to form intermediate phases. XRD result of heat-treated sample A at 500 °C in Fig. 6 reveals that these intermediate phases are Al_3Ti and Ti_2O_3 together with Al_2O_3 produced as a result of partial reduction of TiO_2 by Al. Formation of intermediate phases in the first step of the reaction may decrease the reaction rate. Therefore,

Table 2 Thermal analysis data of A, B3, and C3 samples

Sample	T_{on} (°C)	$T1_{max}$(°C)	$T2_{max}$(°C)	A (J/g)
A	540	584	612	228
B3	540	592	642	268
C3	540	595	–	133

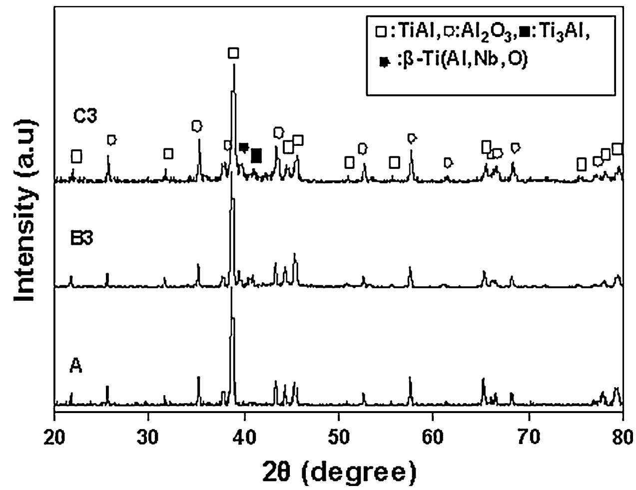

Fig. 5 XRD patterns of A, B3, and C3 samples milled for 8 h and heat treated at 700 °C

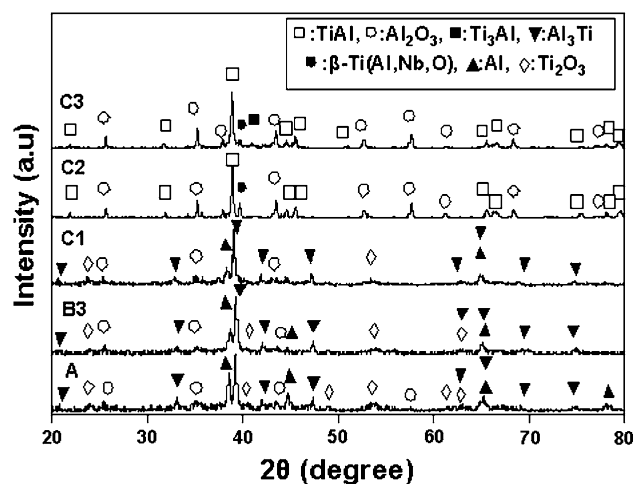

Fig. 6 XRD patterns of A, B3, and C1–C3 samples milled for 8 h and heat treated at 500 °C

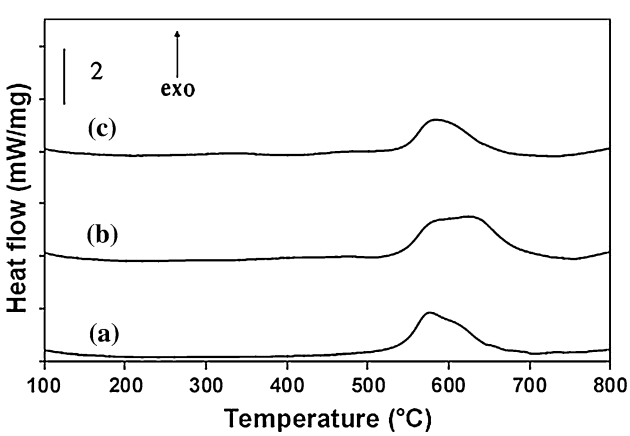

Fig. 4 DTA curves of the (*a*) A, (*b*) B3, and (*c*) C3 samples after 8 h of milling

progress of the second step of the reaction through intermediate phases for formation of the final products requires higher activation energies. Therefore, a higher temperature is needed to complete the reaction. The second exothermic peak is formed at this step with $T2_{max}$ of 612 °C on DTA trace and as a result TiAl and Al_2O_3 are produced. The following reaction sequence may be assumed during the heat treatment of sample A.

$$3TiO_2 + 7Al \rightarrow Al_3Ti + Ti_2O_3 + Al_2O_3 + 2Al \rightarrow 3TiAl + 2Al_2O_3 \quad (4)$$

DTA trace of sample B3 in Fig. 4b is again a combination of two exothermic peaks. The mechanism of reaction progress is indeed similar to the sample A. However, in contrast with the sample A, the exothermic reactions occur at higher temperatures of $T1_{max}$ of 592 °C and $T2_{max}$ of 642 °C. This could be explained by the presence of high amount of Nb in the matrix which decreases diffusion rate of atoms; therefore, the reaction progress needs higher activation energy. As it was explained in Sect. Milling stage, dissolution of Nb in Al matrix increases the melting point of Al. In a certain crystalline structure, self diffusion coefficient in melting point is a constant value. Therefore, if addition of an element increased the melting point, the self diffusion coefficient would be declined in a certain temperature and vice versa [31]. Hence, Nb additions reduce the self diffusion coefficient of Al.

It can be seen in Table 2 that the peak area in sample B3 is higher than other samples. As discussed earlier on Fig. 3, higher introduced internal energy resulted in higher grain refinement in sample B3 compared to other samples; therefore, the higher exothermicity in this sample may be explained by the stress relaxation and nano-crystalline growth. In addition, the higher exothermicity may be contributed to the decomposition of solid solution which is also an exothermic process.

In the case of Nb_2O_5 addition, DTA trace of sample C3 in Fig. 4c does not show the combined exothermic peaks. This could be explained by the possibility of a reaction between Nb_2O_5 with Al to form Nb and Al_2O_3 as follows:

$$3Nb_2O_5 + 10Al \rightarrow 6Nb + 5Al_2O_3 \quad (5)$$

This exothermic reaction takes place simultaneously with the reaction (1); therefore, unlike the samples A and B3, the exothermicity of these two sub-reactions accelerates the reaction rate. The XRD pattern of the sample C3 in Fig. 6 supports this point as the final phases were formed even at 500 °C in this sample.

Although Nb_2O_5 addition does not change the lattice parameter or grain size of Al during the milling process, its presence accelerates the reaction kinetics during heat treatment. Increased fresh interfaces between reactants, which facilitate the nucleation of product phases, are just one of the reasons. Reduced distances between oxide particles are also effective in acceleration of the reaction kinetics.

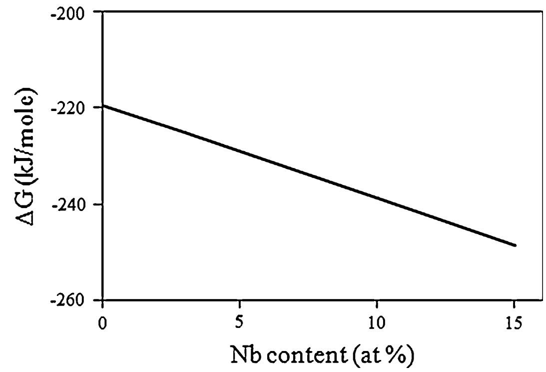

Fig. 7 Gibbs free energy changes as a function of Nb content in samples C1–C4 at 500 °C

Moreover, the presence of Nb_2O_5 in the powder mixture decreases the Gibbs free energy of the reaction. Figure 7 represents the Gibbs free energy changes as a function of Nb content in the powder mixtures containing different amounts of Nb_2O_5 at 500 °C. It reveals that the addition of Nb_2O_5 decreases the free energy of formation of the composite. It could be observed in the XRD patterns in Fig. 6 that increasing the amount of Nb_2O_5 in the starting powder from 2.77 wt% in sample C1 to 4.59 wt% in sample C2 causes the reaction to take place in a single stage at 500 °C.

It is interesting to note that addition of Nb regardless of its source leads to the presence of Ti_3Al phase in the final product since Nb is a Ti_3Al stabilizer in Ti–Al system.

Figure 8 shows the calculated mean crystallite size of TiAl phase after heat treatment of the samples at 700 °C. The results reveal that Nb additions cause the refinement in crystallite size of TiAl matrix in the composite structure. It could be observed that irrespective of how Nb is added to

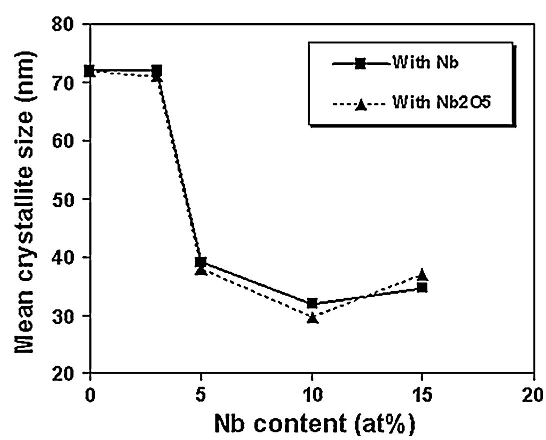

Fig. 8 Mean crystallite size of TiAl as a function of Nb content in samples milled with different additives and heat treated at 700 °C

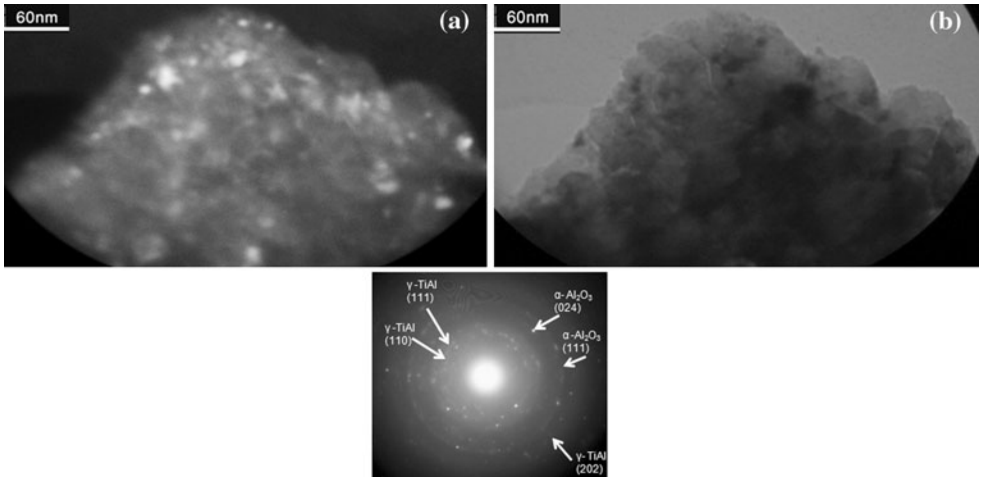

Fig. 9 TEM images of the sample C3 obtained after 8 h milling and heat treatment at 700 °C: **a** bright-field image and **b** dark-field image obtained using (024) Al_2O_3 reflection

the compound; the obtained crystallite sizes are only dependent on the Nb content in the system. Up to 3 at% Nb, the reduction in crystallite size is negligible. Increasing the Nb content to 5 at% significantly decreases the crystallite size. More increase in Nb content has again no considerable effect on the crystallite size of TiAl matrix in the composite.

Although synthesis of the Nb-containing nano-composite is beneficial in terms of attaining a finer crystallite size, usage of Nb_2O_5 as the Nb source seems to be more advantageous since it accelerates the reaction and the nano-composite is formed at lower temperatures and in a single stage.

In order to investigate the microstructure of the final nano-composite produced in the presence of Nb_2O_5 additive, TEM technique was used. Figure 9 shows TEM images with its corresponding selected area diffraction (SAD) pattern of the sample C3 obtained after 8 h mechanical alloying and heat treatment at 700 °C. Both bright-field and dark-field images confirm a nano-crystalline structure of TiAl with a mean crystallite size of around 30 nm, which is in good agreement with the calculated results obtained from the XRD data analysis. This structural refinement into nanometer scale is further evinced by the continuous circular SAD pattern inset in Fig. 9b. It is evident that nano-sized Al_2O_3 is uniformly dispersed all over the TiAl matrix.

Conclusions

In this research, the effect of Nb and Nb_2O_5 additives on formation of $TiAl/Al_2O_3$ nano-composite via mechanical activation of TiO_2 and Al powder mixture and subsequent heat treatment was investigated. The results revealed that during 8 h of milling, no reaction took place even in the presence of Nb and Nb_2O_5. However, Nb was partially dissolved in Al matrix. In addition, Nb additions significantly reduced the crystallite size of Al during milling process, whereas Nb_2O_5 addition had almost no effect on the crystallite size. It was found that the reaction mechanism during heat treatment of the milled sample without any additives is similar to the sample milled in the presence of Nb. It means Al_3Ti and Ti_2O_3 appeared as intermediate phases in a two-stage process. However, Nb_2O_5 addition leads to rapid progress of the reaction in one stage. The reason may be related to the simultaneous reduction of TiO_2 and Nb_2O_5 by Al. Both additives, facilitated formation of useful Ti_3Al phase in the TiAl matrix as Nb is a Ti_3Al stabilizer. The XRD results revealed that both additives refine the size of crystallites in the matrix to about 30 nm which was additionally confirmed by TEM investigation.

Acknowledgements The financial support of this study by the Iran National Science Foundation and Iran Nanotechnology Initiative Council is gratefully acknowledged.

References

1. Nowak R, Lanata T, Sobczak N, Ricci E, Giuranno D, Novakovic R, Holland-Moritz D, Egry I (2010) J Mater Sci 45:1993. doi:10.1007/s10853-009-4061-z
2. Simões S, Viana F, Ventzke V, Kocak M, Ramos AS, Vieira MT, Vieira MF (2010) J Mater Sci 45:4351. doi:10.1007/s10853-010-4303-0
3. Zan X, He Y, Wang Y, Lu Z, Xia Y (2010) J Mater Sci 45:6446. doi:10.1007/s10853-010-4730-y
4. Chen SH, Mukherji D, Schumacher G, Frohberg G, Wahi RP (2001) Mater Sci Eng A300:299
5. Vojtěch D, Čížkovský J, Novák P, Šerák J, Fabián T (2008) Intermetallics 16:896

6. Ward-Close CM, Minorb R, Doorbarb PJ (1996) Intermetallics 4:217
7. Brunet A, Valle R, Vassel A (2000) Acta Mater 48:4763
8. Welham NJ (1998) Mater Sci Eng A255:81
9. Travitzky N, Gotman I, Claussen N (2003) Mater Lett 57:3422
10. Ying DY, Zhang DL, Newby M (2004) Metall Mater Trans A 35A:2115
11. Fana R, Liu B, Zhang J, Bi J, Yin Y (2005) Mater Chem Phys 91:140
12. Kleiner S, Bertocco F, Khalid FA, Beffort O (2005) Mater Chem Phys 89:362
13. Gaus SP, Harmer PH, Chan HM (2000) J Am Ceram Soc 83:1606
14. Feng CF, Froyen L (2000) Composites A 31:385
15. Bououdina M, Luklinska Z, Guo ZX (2008) Mater Sci Eng A 474:173
16. Cao R, Zhu H, Hong Chen J, Zhang J (2008) J Mater Sci 43:299. doi:10.1007/s10853-007-2172-y
17. Cao GH, Liu ZG, Shen GJ, Liu JM (2001) J Alloys Compd 325:263
18. Song Y, Xu DS, Yang R, Li D, Hu ZQ (1998) Intermetallics 6:157
19. Sawai T, Wakai E, Jitsukawa S, Hishinuma A (2002) J Nucl Mater 307–311:389
20. Kawabata T, Fukai H, Izumi O (1998) Acta Mater 46:2185
21. Zhang XJ, Gao YH, Ren BY, Tsubaki N (2010) J Mater Sci 45:1622. doi:10.1007/s10853-009-4138-8
22. Yuan Y, Liu HW, Zhao XN, Meng XK, Liu ZG, Boll T, Al-Kassab T (2006) Phys Lett A 358:231
23. Bystrzanowski S, Bartels A, Clemens H, Gerling R, Schimansky FP, Dehm G, Kestler H (2005) Intermetallics 13:515
24. Hao YL, Yang R, Cui YY, Li D (2000) Acta Mater 48:1313
25. Klug HP, Alexander L (1974) X-ray Diffraction Procedures for Poly-Crystalline and Amorphous Materials. JWiley, New York
26. Cullity BD (1978) Elements of X-Ray Diffraction. Addison-Wesely Publishing Co., USA
27. (Sam) Froesa FH, Suryanarayana C, Russell K, Li CG (1995) Mater Sci Eng A 192–193:612
28. Al-Aqeeli N, Mendoza-Suarez G, Suryanarayana C, Drew RAL (2008) Mater Sci Eng A 480:392
29. Suryanarayana C (2001) Prog Mater Sci 46:1
30. Okuno K, Yamashita H, Oida K, Nishikawa O (1987) J Phys C6 48:511
31. Porter DA, Easterling KE (1995) Phase transformations in metals and alloys. Chapman & Hall, London